On a Class of Predefined Wavelet Packet Bases for Efficient Representation of Electromagnetic Integral Equations

Hai Deng, *Student Member, IEEE*, and Hao Ling, *Fellow, IEEE*

***Abstract*— A general wavelet packet tree is proposed to design predefined wavelet packet (PWP) bases for the efficient representation of electrodynamic integral equations. The wavelet packet decomposition tree is constructed by zooming in along the spectral oscillatory frequency of the free-space Green's function. Numerical results show that for typical two-dimensional (2-D) scatterers the number of above-threshold elements in the PWP-based moment matrix is on the order of $O(N^{1.3})$ and tends to grow at a rate of $O(N \cdot \log N)$ for large-scale problems. Therefore, the complexity of solving the moment equations can be reduced accordingly. Furthermore, it is shown that the elements of the moment matrix based on the PWP bases can be computed directly at approximately the same complexity as the fast wavelet transform approach. Consequently, with on-the-fly thresholding of the matrix elements, the $O(N^2)$ memory bottleneck in the formation of the PWP-based moment matrix can be circumvented.**

***Index Terms*—Boundary integral methods, wavelet transforms.**

I. Introduction

RECENTLY there has been much research interest in applying wavelet basis to sparsify the method-of-moments matrix to reduce the complexity of solving electromagnetic integral equations [1]–[10]. For integral equations with smooth kernel functions such as those found in electrostatics, the nonzero elements of the transformed matrix can be sparsified to the order of $O(N \cdot \log N)$ using the conventional wavelet transform [11]. However, when it is applied to electrodynamic integral equations, the transformed matrices still have about $O(\beta N^2)$ $(0<\beta<1)$ nonzero elements [5], [10]. The conventional wavelet basis has constant Q property and, thus, is well suited for representing smooth signals in which the component with the longest spatial extent has the lowest spectral frequency. As we have reported in [7], [9], [10], since the Green's function in electromagnetic integral equations is oscillatory at the spectral frequency k_0, a more efficient way to represent moment matrix is to choose a wavelet basis to reflect the oscillatory nature of the Green's function.

The application of wavelet packet basis for moment matrix sparsification has recently been introduced into the electromagnetics community. Baharav and Leviatan found a wavelet packet basis to compress moment matrix based on the physical optics current [6]. Golik investigated wavelet packet basis selection through the decomposition of the excitation vector of the moment equation [8]. We have applied the adaptive wavelet packet transform (AWPT) method to find the optimal wavelet packet basis by choosing the sparsity of the transformed moment matrix as the cost function [9], [10]. By adaptively searching for the optimal wavelet packet basis for each scatterer, we found that the nonzero elements in the transformed moment matrix grow at a rate of $N^{1.4}$. Consequently, the computational complexity of solving the resulting equation via an iterative solver is significantly reduced. One drawback of the AWPT algorithm is that additional computation cost is needed to find the best wavelet basis. In addition, the original moment matrix must be generated first before the best basis search and transformation can be carried out. This introduces an $O(N^2)$ memory requirement to store the original moment matrix elements and makes the numerical implementation very memory-intensive. In this paper, we set out to find a class of efficient wavelet packet bases that is scatterer-independent to eliminate the scatterer-dependent search procedure for the best basis. Furthermore, we set out to overcome the N^2 memory bottleneck without increasing the computation complexity of the procedure.

As we have observed in [10], the optimal wavelet packet decomposition trees for different scatterers tend to grow near the branch that corresponds to the free-space wave number k_0 and are relatively insensitive to the physical structure of the scatterers. This observation is consistent with the oscillatory nature of the Green's kernel and motives us to propose a class of wavelet packet decomposition trees that is applicable for moment matrix sparsification of arbitrary scatterers. The proposed tree grows along the spectral frequency k_0 rather than along the lowest frequency as in the conventional wavelet transform. This implies that the basis functions with the longest spatial extent in the basis set are oscillatory at the spectral frequency k_0. Since this kind of wavelet packet basis is predetermined based on our knowledge of the Green's kernel, we shall term it the predefined wavelet packet (PWP) basis [12]. The PWP basis can be designed easily for a given problem size without any extra computation cost to search out the optimal basis. We find the new PWP bases lead to moment systems that are as sparse as those obtained with the adaptive wavelet packet transform for small-size

Manuscript received November 5, 1998; revised September 2, 1999. This work was supported by the Air Force MURI Center for Computational Electromagnetics under contract AFOSR F49620-96-1-0025 and in part by the Joint Services Electronics Program under contract AFOSR F49620-95-C0045.

The authors are with the Department of Electrical and Computer Engineering, The University of Texas at Austin, Austin, TX 78712-1084 USA.

Publisher Item Identifier S 0018-926X(99)09978-0.

problems. For larger size problems $(N > 1000)$, the PWP-based systems are even sparser. With the PWP basis in place, we next devise an implementation to calculate the moment matrix elements directly from the PWP basis functions. By exploiting the finite support property of the PWP bases, it is possible to implement such calculations at a similar computational complexity level as the fast transformation method. By thresholding the elements on-the-fly, we can achieve the goal of overcoming the N^2 bottleneck in memory.

This paper is organized as follows. In Section II, we introduce the wavelet packet basis concept and detail the design of the PWP basis for efficient moment matrix representation. In Section III, we discuss the implementation methods for the calculation of moment matrix elements from the PWP basis functions. In Section IV, we present numerical results based on several typical two-dimensional (2-D) scatterers. Some conclusions are given in Section V.

II. Wavelet Packet Basis and PWP Basis Design

Wavelet packet basis consists of a set of multiscale functions derived from the shift and dilation of a basic wavelet function. The wavelet packet basis space is generated from the decomposition of both the scaling function space and the corresponding basic wavelet function space. Note that the conventional wavelet basis space can be considered as a special case of the wavelet packet space when the decomposition takes place only in the scaling function space [13]–[15]. Let us assume that $\psi(x)$ is the wavelet packet basis function with the finest spatial resolution available for signal analysis. Using the "two-scale equations" we can express the wavelet packet basis functions in the next scale as [15]

$$\psi_0^1(n) = \sum_k \psi(k) h(2n-k)$$
$$\psi_1^1(n) = \sum_k \psi(k) g(2n-k) \tag{1}$$

where $\{h(k)\}$ and $\{g(k)\}$ are the impulse responses of two quadrature filters H (low-pass) and G (high-pass), respectively. The functions in the next scale become coarser in spatial resolution and finer in spectral resolution through filtering and down sampling in (1). The same procedure can be applied recursively to the outputs of (1) into subsequent scales. Conversely, the decomposition results in (1) can be used to reconstruct the original sequence by using another pair of quadrature filters P and Q. This reconstruction or synthesis procedure can be expressed as

$$\psi(x) = \sum_k p(x-2k)\psi_0^1(k) + \sum_k q(x-2k)\psi_1^1(k) \tag{2}$$

where $\{p(k)\}$ and $\{q(k)\}$ are the impulse responses of P (low-pass) and Q (high-pass), respectively. The functions become finer in spatial resolution and coarser in spectral resolution through filtering and up-sampling in (2).

A complete and orthogonal wavelet packet basis can be generated from a frequency decomposition tree which starts from an initial function $\psi(x)$ with the finest spatial resolution by using recursive two-channel filtering and down-sampling in (1). It can be shown that the decomposed functions at the outermost branches of the tree satisfy orthogonality and completeness for any decomposition trees and, thus, constitute a wavelet packet basis set [10], [14]. Our goal is to generate a special wavelet packet tree and the corresponding wavelet packet basis, to efficiently represent the moment matrix. In the proposed wavelet packet tree, the two-channel decomposition zooms in along the oscillatory spectral frequency k_0. The wavelet packet basis corresponding to this type of tree forms our PWP basis. Fig. 1(a) and (b) shows, respectively, the conventional wavelet decomposition tree and the PWP decomposition tree for $N = 32$. Note that the former always zooms in along the low-frequency branch while the latter zooms in along a preselected frequency. We shall describe each tree by a data sequence that follows the depth indexes on the outermost branches of the tree from the lowest frequency to the highest one [14]. Therefore, the conventional wavelet basis in Fig. 1(a) can be represented by $\{5,5,4,3,2,1\}$ and the PWP basis in Fig. 1(b) by $\{3,4,5,5,2,1\}$.

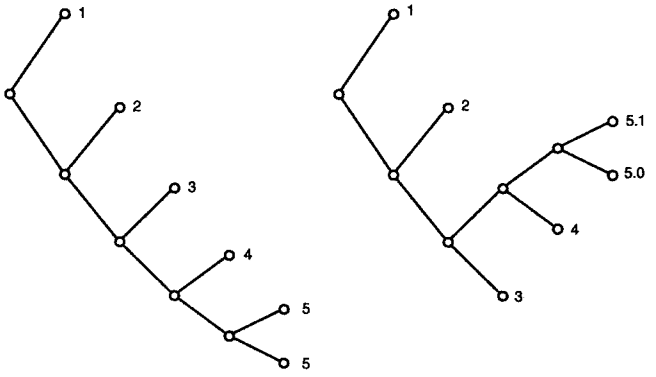

(a) (b)

Fig. 1. (a) Conventional wavelet decomposition tree. (b) Wavelet packet decomposition tree.

The zoom-in frequency in the PWP decomposition tree is derived from the oscillation frequency of the Green's function $k_0 = 2\pi/\lambda$ and the spatial discretization interval in the moment equations. If a standard spatial discretization interval of $\lambda/10$ is assumed, the highest spectral frequency in the moment matrix data is $10k_0$. This corresponds to a normalized frequency of 2π. Since the wavelet packet decomposition tree ranges from 0 to π, the oscillatory frequency k_0 should correspond to a normalized frequency of $\pi/5$. Hence, the PWP basis design criterion is to try to find a wavelet packet decomposition tree such that the center frequency of its deepest branch is as close as possible to $\pi/5$ in the spectral domain.

Fig. 2 illustrates how the PWP decomposition tree is constructed for $N = 16$. Every node in the tree is labeled with a number that denotes the layer of the node and the sequential number of this node within the layer. Noting the two-channel decomposition filtering, we can derive the center frequencies

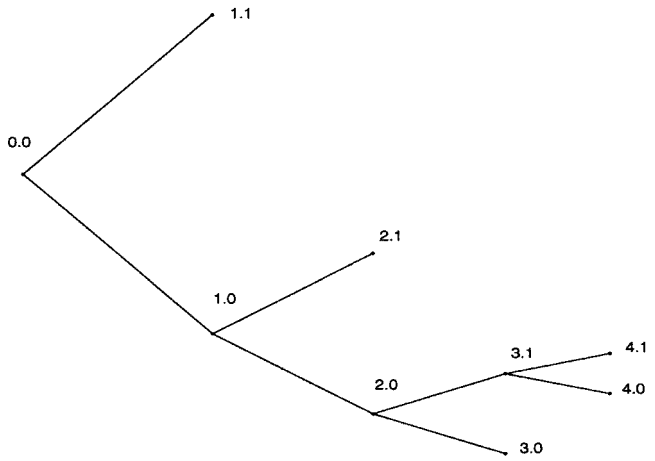

Fig. 2. Design of the PWP decomposition tree with $N = 16$.

of the functions corresponding to the nodes as follows:

$$\begin{array}{llll} \text{Node } 0.0: & f_c = \pi/2 & \text{Node } 3.0: & f_c = \pi/16 \\ \text{Node } 1.0: & f_c = \pi/4 & \text{Node } 3.1: & f_c = 3\pi/16 \\ \text{Node } 1.1: & f_c = 3\pi/4 & \text{Node } 4.0: & f_c = 5\pi/32\,. \\ \text{Node } 2.0: & f_c = \pi/8 & \text{Node } 4.1: & f_c = 7\pi/32 \\ \text{Node } 2.1: & f_c = 3\pi/8 & & \end{array}$$

In this case, Node 4.1 is the node in the tree with a center frequency closest to $\pi/5$. Following the same logic, we can synthesize the PWP basis for problems of arbitrary size. For instance

$$\begin{aligned} &\mathrm{N} = 4 \quad \text{PWP Basis} = \{2,2,1\} \\ &N = 8 \quad \text{PWP Basis} = \{3,3,2,1\} \\ &N = 16 \quad \text{PWP Basis} = \{3,4,4,2,1\} \\ &N = 32 \quad \text{PWP Basis} = \{3,4,5,5,2,1\} \\ &N = 64 \quad \text{PWP Basis} = \{3,4,6,6,5,2,1\} \\ &N = 128 \quad \text{PWP Basis} = \{3,4,7,7,6,5,2,1\} \\ &N = 256 \quad \text{PWP Basis} = \{3,4,7,8,8,6,5,2,1\} \\ &\qquad \cdots\cdots \end{aligned}$$

The corresponding PWP decomposition trees for $N = 4, 8, 16, 32, 64$, and 128 are shown in Fig. 3.

With the PWP basis decomposition tree in place, the actual PWP basis functions can theoretically be obtained by feeding the tree with the scaling function as the input signal [16]. The output functions at the outermost nodes in the tree are then the PWP basis functions. However, in actual implementation the determination of the scaling function is not straightforward. We instead make the observation that the outputs of the PWP decomposition tree are equivalent to the projections of the input function on the orthogonal PWP basis functions. If a PWP basis function is used as the input to the PWP decomposition tree, the output from the branch corresponding to that basis function is exactly one while all other outputs are zeros. Hence, we can reconstruct the ith PWP basis function by a PWP synthesis tree with an input data sequence $[0, 0, \cdots, 0, 1, 0, \cdots, 0, 0]$, in which the ith datum is "1" and all others are zeros. The PWP synthesis trees are the same as the decomposition trees shown in Fig. 3, except that the input data are fed from the right-hand side and the processing is that of convolution and up-sampling using quadrature filters P and Q as described in (2). For moment equations of size of N, the general procedure to calculate the PWP basis functions is as follows.

1) Construct the PWP wavelet packet decomposition tree with $\log_2 N$ layers. The two-channel decomposition always zooms in along the spectral frequency k_0.
2) Construct the PWP synthesis tree by inverting the decomposition tree with a pair of synthesis filters P and Q.
3) Input the data sequence with a single "1" and the rest "0" to the synthesis tree and use (2) to reconstruct the PWP basis function corresponding to the "1" in the input sequence.
4) Find all other PWP basis functions by changing the position of "1" in the input sequence in Step 2.

Fig. 4 shows the PWP basis functions with a problem size of 128. They are calculated from the Daubechies wavelet filters with order 16 using the procedure described above. The total number of PWP basis functions should be the same as the problem size. However, only one basis for each scale is shown, since bases within the same scale differ only by spatial shifts. Note that the basis in Fig. 4(c) has the longest spatial extent and oscillates at a spectral frequency closest to k_0.

III. Calculation of Moment Matrix Represented with PWP Basis

The moment equation with the PWP basis as expansion and testing functions is defined as follows:

$$\tilde{\boldsymbol{Z}} \cdot \tilde{\boldsymbol{J}} = \tilde{\boldsymbol{E}} \tag{3}$$

where $\tilde{\boldsymbol{Z}}, \tilde{\boldsymbol{J}}$, and $\tilde{\boldsymbol{E}}$ are the moment matrix, induced current vector, and incident excitation vector under the PWP basis, respectively. We need to compute $\tilde{\boldsymbol{Z}}$ and $\tilde{\boldsymbol{E}}$ first and find $\tilde{\boldsymbol{J}}$ by solving (3).

One method to compute the moment matrix $\tilde{\boldsymbol{Z}}$ under the wavelet packet basis is to first generate the moment matrix $\boldsymbol{Z}$ in the standard subsectional basis and then transform $\boldsymbol{Z}$ into $\tilde{\boldsymbol{Z}}$. The transformation can be efficiently implemented with the filtering and down-sampling via a two-channel filter bank structure similar to (1). In this case, the input data to the filter bank is the original moment matrix $\boldsymbol{Z}$ in the space domain, which can be considered as the sampled signal with the finest spatial resolution. The transformation is carried out according to the PWP decomposition designed in the last section. The final output is the transformed moment matrix in the PWP basis. The reader is referred to [10] for a detailed description on its implementation. The computation complexity of the fast transformation method is $O(N^2 \cdot \log N)$ for a full decomposition basis, and is about $O(N^2)$ for a single-

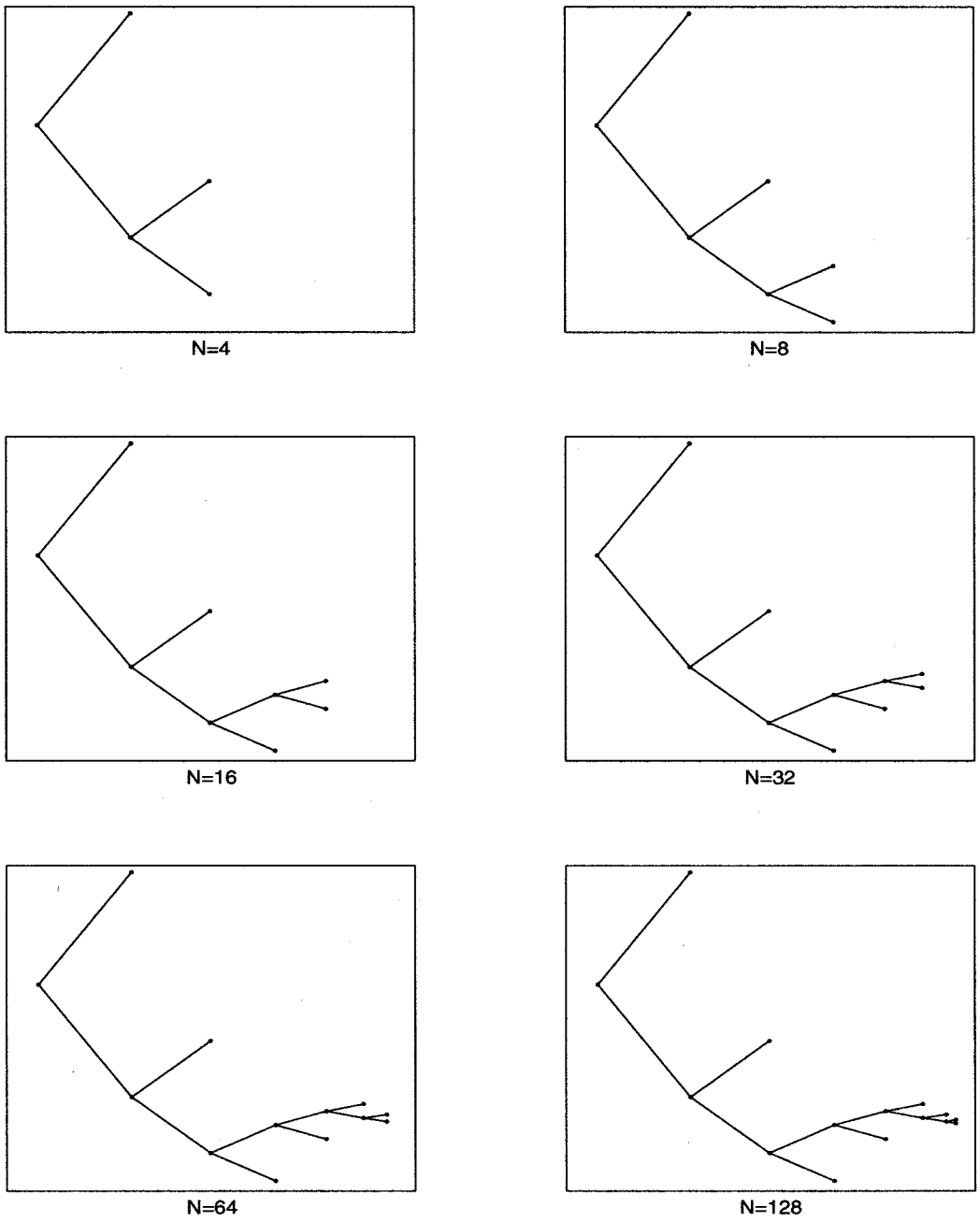

Fig. 3. PWP decomposition trees for $N = 4, 8, 16, 32, 64,$ and 128.

frequency zoom-in basis like the PWP basis. The total memory required to implement the transform method scales as $O(N^2)$ since the dense moment matrix in the space domain must first be computed. This presents a key drawback for solving large-scale problems.

Another way to find the moment matrix in the PWP basis is to calculate each element of the matrix from the PWP basis functions directly. Since the resulting matrix is expected to contain a small number of nonnegligible elements, only those significant elements need to be stored. Therefore, this approach presents a way to overcome the N^2 bottleneck in memory. Assuming that data sequences $\{\mu_m(k)\}$ and $\{\mu_n(l)\}$ are two of the PWP basis functions, we can compute the element of the moment matrix $\tilde{Z}$ directly as

$$\tilde{Z}(m,n) = \sum_k \sum_l \mu_m(k) K(k,l) \mu_n(l) \tag{4}$$

where $K(k,l)$ is the discretized Green's kernel in the electromagnetic integral equation. For 2-D combined field integral equations (CFIE), the kernel function $K(k,l)$ can be approximated as (5) [17], shown at the bottom of the next page, where δ is the discretization interval of the pulse basis, $\mathbf{r}_k$ and $\hat{n}_k$ are the position vector, and the outward pointing normal of the sampling point k on the scatterer boundary. ρ is the combination parameter of the CFIE, γ is Euler's constant, and $H_p^{(2)}$ is Hankel function of the second kind of order p. The

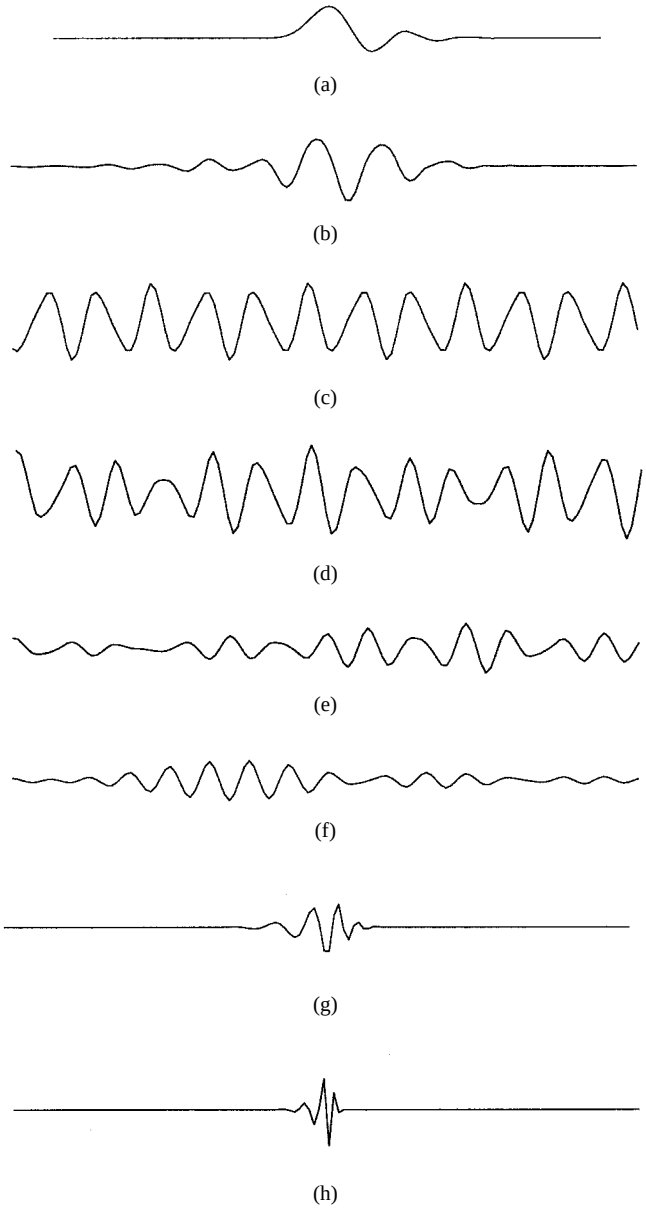

Fig. 4. The PWP basis functions with $N = 128$. The functions (a)–(h) correspond to the nodes in the PWP decomposition tree for $N = 128$ in Fig. 3 from the lowest node to the highest node.

impedance matrix element $\tilde{\boldsymbol{Z}}(m,n)$ can then be interpreted as the projection of the 2-D kernel function $K(k,l)$ onto $\mu_m(k)$ and $\mu_n(l)$.

Once $\tilde{\boldsymbol{Z}}$ is computed, the remaining procedure is straightforward. We first obtain the excitation vector $\tilde{\boldsymbol{E}}$ in (3) from the original excitation vector by two-channel decomposition with the quadrature filters H and G based on the PWP basis. Then the induced current $\tilde{\boldsymbol{J}}$ can be solved by using an iterative solver

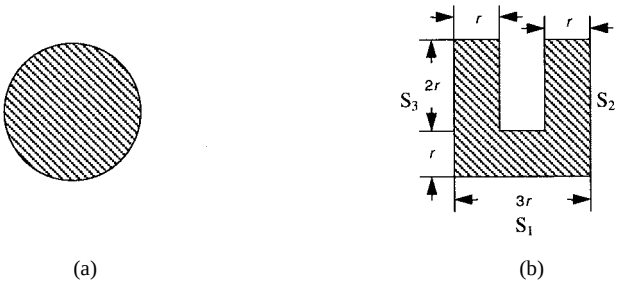

Fig. 5. Geometries of the test targets. (a) A circular cylinder. (b) A duct.

with a complexity proportional to the number of nonzero elements in the PWP moment matrix $\tilde{\boldsymbol{Z}}$. Finally, the original induced current $\boldsymbol{J}$ can be restored from $\tilde{\boldsymbol{J}}$ by using the inverse wavelet packet transform with the quadrature filters P and Q based on the same PWP basis.

IV. Numerical Results

Two 2-D scatterers, a circular cylinder, and a duct (shown in Fig. 5) are used to test the effectiveness of the PWP basis in sparsifying the method of moment matrix. The combined field integral equation (CFIE) is used to formulate the problem in terms of the induced surface currents on the scatterers under TM polarized incidence. The PWP basis functions are derived from the Daubechies filter of order 16 (with seven vanishing moments) using the algorithm described in Section II. The perimeters of the scatterers in Fig. 5 are changed from 12.8λ to 819.2λ, while the spatial discretization interval is kept fixed at 0.1λ. Thus, the size N of the electromagnetic problems varies from 128 to 8192. With the moment matrix $\tilde{\boldsymbol{Z}}$ in PWP basis, an absolute threshold level ε is applied to all entries of $\tilde{\boldsymbol{Z}}$ to make it sparse. Experimentation shows that if we choose a fixed threshold $\varepsilon = 1.5$ for the duct scatterer and $\varepsilon = 0.5$ for the circular cylinder scatterer, the calculated induced current has an root-mean square (rms) error of around 3%, which is close to the results obtained using adaptive thresholds based on moment matrix norms [10]. Fig. 6(a) and (b) show the thresheld PWP moment matrices for $N = 512$ for the circular cylinder and the duct, respectively. The lower right corners of the matrices represent the strength of electromagnetic interactions between PWP bases of high spectral frequency and small spatial extent, resembling those shown in Fig. 4(g) and (h). As we move closer to the upper left corners of the matrices, the elements represent the interactions between PWP bases with longer spatial extent. The bases with the longest spatial extent have spectral frequency close to k_0, resembling that shown in Fig. 4(c). Fig. 7(a) shows the induced currents on the boundary of the duct scatterer calculated from the thresheld PWP moment matrix for $N =$

$$K(k,l) = \begin{cases} \dfrac{\omega\mu_0\delta}{4}\left[1 - j\dfrac{2}{\pi}\ln\left(\dfrac{e^{\gamma}k_0\delta}{4e}\right)\right] + \rho/2 & (k = l) \\ \dfrac{\omega\mu_0\delta}{4}\left[H_0^{(2)}(k_0|\mathbf{r}_k - \mathbf{r}_l|) + \rho k_0\left(\hat{n}_k \cdot \dfrac{\mathbf{r}_k - \mathbf{r}_l}{|\mathbf{r}_k - \mathbf{r}_l|}\right)H_1^{(2)}(k_0|\mathbf{r}_k - \mathbf{r}_l|)\right] & (k \neq l) \end{cases} \tag{5}$$

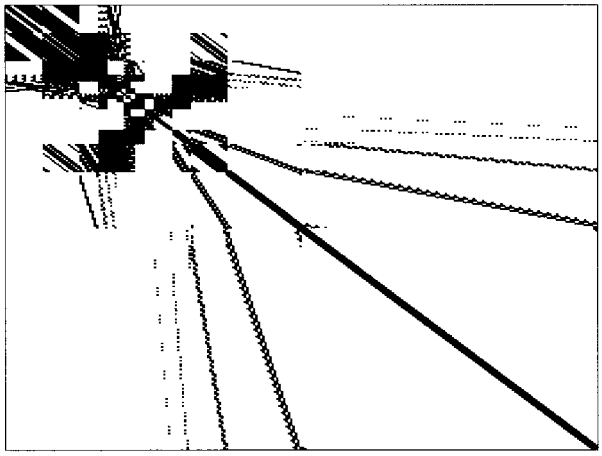

(a)

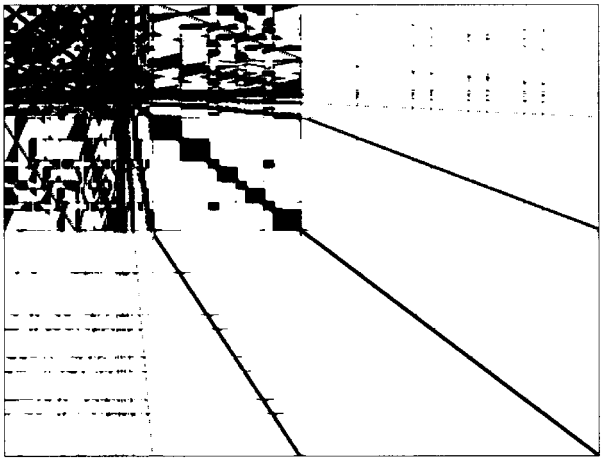

(b)

Fig. 6. The PWP-based moment matrices with $N = 512$ for (a) the circular cylinder and (b) the duct.

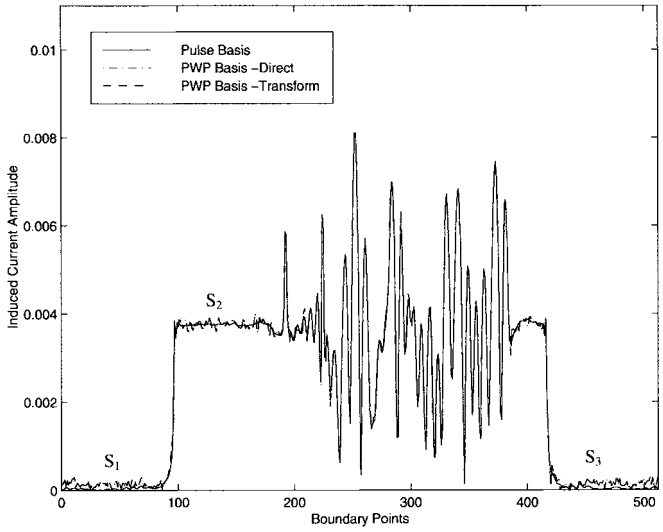

(a)

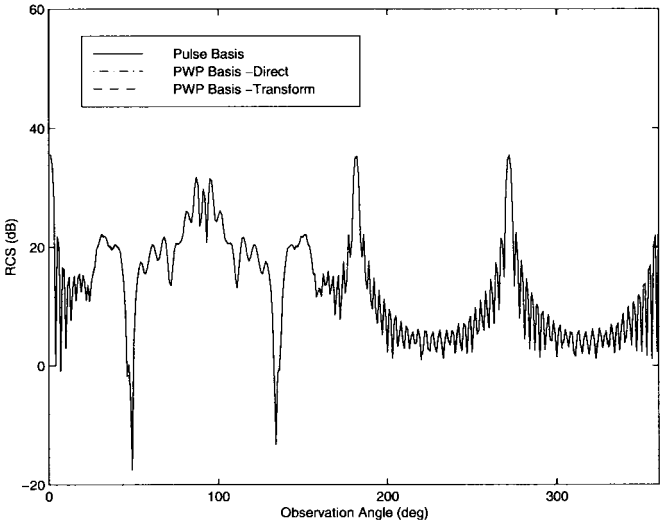

(b)

Fig. 7. (a) Induced current distribution and (b) RCS solved using the PWP basis with the direct calculation and basis transform methods for the duct with $N = 512$. The incident wave is E_Z-polarized at 45° from the duct opening. The exact solutions using regular pulse basis are also plotted for reference.

512. The excitation is an E_z-polarized plane wave incident from 45° into the duct. Fig. 7(b) displays the radar cross section (RCS) curves calculated from the induced currents on the duct. The PWP moment matrices are calculated using both the fast transform method and the direct calculation method described in Section III. For reference, the current and RCS calculated from the standard moment equation with pulse basis and point matching are also plotted in the same figures. The induced currents computed by solving the PWP-based system with threshold result in about a 3.2% rms error when compared against the reference result. The two different methods to compute the PWP moment matrix gave nearly the same results, with only a 0.25% rms difference between the two induced currents. The RCS curves in Fig. 7(b) show that the PWP results are nearly indistinguishable from the reference result. Similar induced current and RCS results are obtained for the circular cylinder.

Once the accuracy of the PWP scheme is established, we next examine how the sparsity of the PWP matrix scales with problem size. Fig. 8(a) and (b) shows the number of nonzero elements in the thresheld PWP moment matrix versus problem size for the circular cylinder and the duct, respectively. Also plotted in dashed lines are the $O(N^2)$ and $O(N \cdot \log N)$ curves for reference. We find the nonzero elements grow at a rate of about $N^{1.3}$ for N less than 1024, but the growth rate appears to approach $(N \cdot \log N)$ as the problem size gets larger. This observation applies to both the smooth cylinder and the more complex duct shape. We have also tried different choices of wavelet filters and different threshold levels. Results show that while these choices change the absolute sparsity of PWP moment matrices, they do not significantly affect the growth rate of the above-threshold elements in these matrices. Therefore, the computation cost for solving the PWP-based moment equations should approach $O(N \cdot \log N)$ for large-scale problems using an iterative solver.

Next, we compare the fast transform method and the direct calculation method described in Section III to generate the

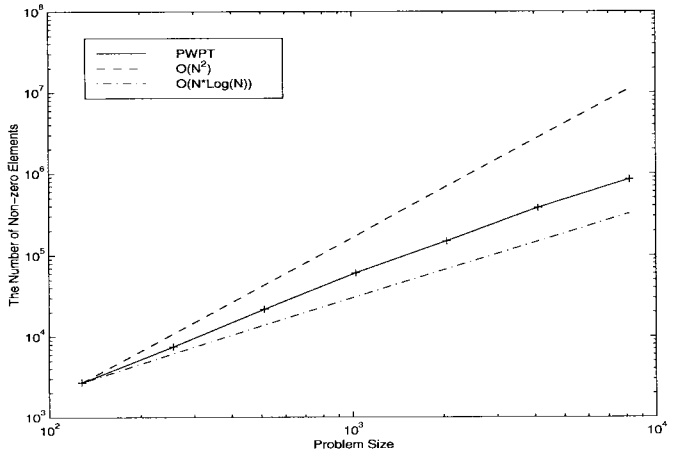

(a)

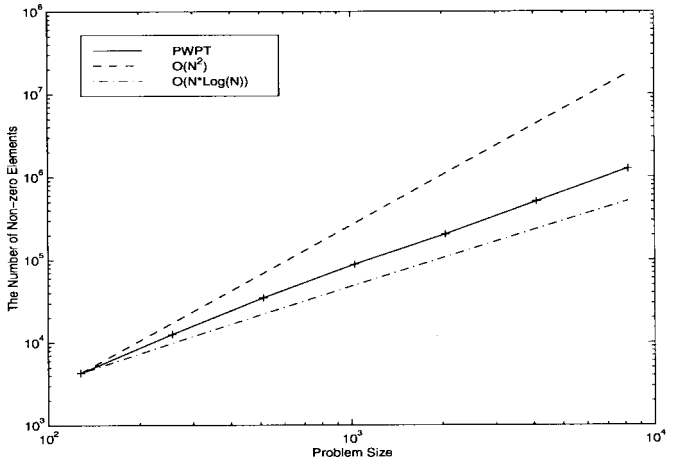

(b)

Fig. 8. The number of nonzero elements in the PWP-based matrices versus problem size N for (a) the circular cylinder and (b) the duct. The N^2 and $(N \cdot \log N)$ curves are plotted in dash line in both figures for reference.

PWP-based moment matrix. We have already shown that these two methods produce almost identical results. The main advantage of using the direct calculation method is that we can overcome the N^2 bottleneck in memory. In the implementation, each calculated moment matrix entry through (4) is compared with the threshold ε. If it is greater than the threshold, its value is kept; otherwise, it is replaced with zero. Because we only need to store those nonzero elements in memory, the total memory requirement for the solution of the integral equation is about the order of the number of the above-threshold elements in the PWP moment matrix, i.e., on the order of $(N \cdot \log N)$.

Finally, we estimate the computational complexity of using the direct calculation method. Since the PWP basis functions have finite support in space, the complexity of the calculation in (4) is proportional to the product of the lengths of the two PWP basis functions. Numerical results show that the average length of all PWP basis functions is approximately on the order of $\log N$. The average complexity for computing each matrix element is thus $(\log N)^2$ and the total complexity of

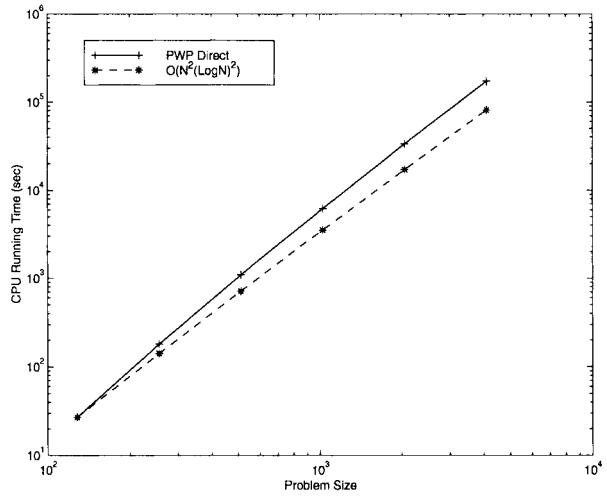

Fig. 9. The CPU run time to fill a PWP moment matrix using the direct calculation method. The time grows approximately at a rate of $N^2(\log N)^2$ versus problem size.

constructing the PWP moment matrix is about $O(N^2(\log N)^2)$ operations. This is only a slight increase in comparison to the complexity of the fast transform method. Fig. 9 shows the actual CPU running time to construct the PWP moment matrix using the direct calculation method. In our direct calculation implementation, a look-up table for the Hankel function is precomputed to speed up the calculation of (4). We observe that the central processing unit (CPU) run time grows at a rate that is quite close to the estimated $N^2(\log N)^2$ curve. Therefore, we can overcome the N^2 memory bottleneck while preserving the time complexity of the fast transform method by using the direct calculation method.

V. Conclusions

We have proposed a general class of PWP basis for the efficient representation of moment matrices arising in electromagnetic integral equations. The PWP basis is constructed from a wavelet packet decomposition tree that zooms in along the spectral oscillatory frequency of the free-space Green's function. This is in contrast to the low frequency zoom-in employed in the conventional wavelet basis. We find that the moment matrix represented by the PWP basis has only about $O(N^{1.3})$ above-threshold elements for small-size problems. For large-size problems, the number of above-threshold elements approaches $O(N \cdot \log N)$. Consequently, the complexity of solving the moment equation can be reduced accordingly when an iterative solver is employed. Compared to the AWPT method we reported earlier, the PWP basis eliminates the need for the costly best basis search, yet its performance is even better than that of the best basis found from the AWPT algorithm. This is because the AWPT basis found is only a locally optimum basis due to computational cost constraints, and the best basis search algorithm becomes less optimal as the problem size increases.

We have also implemented an algorithm to directly calculate the moment matrix elements from the PWP basis functions. Since the elements with amplitude below a threshold

can be eliminated on-the-fly without storage in memory, the maximum memory requirement is on the order of $N^{1.3}$ to $(N \cdot \log N)$ to solve moment equations. This overcomes the N^2 memory bottleneck in the basis transform method where the original space-domain moment matrix must be stored. In the direct calculation method, the finite support of the PWP basis functions is utilized and the computational cost of computing the moment matrix scales approximately as $O(N^2(\log N)^2)$. This is not a significant increase from that required by the fast basis transform method.

While there remains an N^2 computation time bottleneck in the formation of the PWP matrix, we note that the matrix generation is a one-time cost, and yet the cost of solving the resulting matrix equation is amplified by the number of iterations and the number of right-hand sides. Furthermore, we did not take advantage of the vanishing moment property of the wavelet packet basis function in this work. It might be possible to apply the fast-element evaluation technique proposed in [11] to estimate the element amplitude of the PWP moment matrix. If we can accurately predict the position of the elements that are smaller than a predefined threshold, the computation complexity of the direct calculation method could be further reduced. This is a challenging problem for bases with large spatial extent and will need to be further investigated.

REFERENCES

[1] B. Z. Steinberg and Y. Leviatan, "On the use of wavelet expansions in the method of moments," *IEEE Trans. Antennas Propagat.*, vol. 41, pp. 610–619, May 1993.

[2] H. Kim and H. Ling, "On the application of fast wavelet transform to the integral equations solution of electromagnetic scattering problems," *Microwave Opt. Tech. Lett.*, vol. 6, pp. 168–173, Mar. 1993.

[3] K. Sabetfakhri and L. P. B. Katehi, "Analysis of integrated millimeter-wave and submillimeter-wave waveguides using orthonormal wavelet expansion," *IEEE Trans. Microwave Theory Tech.*, vol. 42, pp. 2412–2422, Dec. 1994.

[4] G. Wang and G. Pan, "Full wave analysis of microstrip floating line structures by wavelet expansion method," *IEEE Trans. Microwave Theory Tech.*, vol. 43, pp. 131–142, Jan. 1995.

[5] R. L. Wagner and W. C. Chew, "A study of wavelets for the solution of electromagnetic integral equations," *IEEE Trans. Antennas Propagat.*, vol. 43, pp. 802–810, Aug. 1995.

[6] Z. Baharav and Y. Leviatan, "Impedance matrix compression using adaptively constructed basis functions," *IEEE Trans. Antennas Propagat.*, vol. 44, pp. 1231–1238, Sept. 1996.

[7] H. Kim, H. Ling, and C. Lee, "A fast moment method algorithm using spectral domain wavelet concepts," *Radio Sci.*, vol. 31, pp. 1253–1261, Sept./Oct. 1996.

[8] W. L. Golik, "Wavelet packets for fast solution of electromagnetic integral equation," *IEEE Trans. Antennas Propagat.*, vol. 46, pp. 618–624, May 1998.

[9] H. Deng and H. Ling, "Moment matrix sparsification using adaptive wavelet packet transform," *Electron. Lett.*, vol. 33, pp. 1127–1128, June 1997.

[10] ———, "Fast solution of electromagnetic integral equations using adaptive wavelet packet transform," *IEEE Trans. Antennas Propagat*, to be published.

[11] G. Beylkin, R. Coifman, and V. Rokhlin, "Fast wavelet transforms and numerical algorithms I," *Commun. Pure Appl. Math.*, vol. 44, pp. 141–183, 1991.

[12] H. Deng and H. Ling, "Efficient representation of moment matrix with predefined wavelet packet basis," *Electron. Lett.*, vol. 34, pp. 440–441, Mar. 1998.

[13] R. R. Coifman, Y. Meyer, and M. V. Wickerhauser, "Size properties of wavelet packets," in *Wavelets and Their Applications*. Boston, MA: Jones Bartlett, 1992.

[14] M. V. Wickerhauser, *Adapted Wavelet Analysis from Theory to Software*. Wellesley, MA: Peters, 1994.

[15] C. K. Chui, *An Introduction to Wavelets.* Boston, MA: Academic, 1992.

[16] I. Daubechies, "Orthonormal bases of compactly supported wavelets," *Comm. Pure Appl. Math.*, vol. 41, pp. 909–996, 1988.

[17] C. A. Balanis, *Advanced Engineering Electromagnetics*. New York: Wiley, 1989.

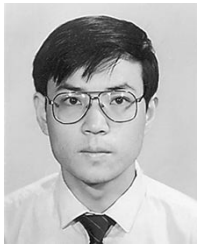

Hai Deng (S'97) was born in Tongcheng, Anhui, China, in 1967. He received the B.S.E.E. degree from Anhui University, China, in 1987, and the M.S.E.E. degree from Beijing Institute of Technology, China, in 1990. He is currently working toward the Ph.D. degree at the University of Texas at Austin.

Since 1996, he has been a Research Assistant in the Electrical and Computer Engineering Department, The University of Texas at Austin. From 1990 to 1996 he was a Design Engineer and later a Senior Engineer at Beijing Institute of Radio Measurement, Beijing, China. His research interests include radar signal processing, wavelet applications to computational electromagnetics, target identification, wilreless communications, and logic and VLSI design.

Hao Ling (S'83–M'86–SM'92–F'99), for photograph and biography, see p. 1453 of the November 1996 issue of this TRANSACTIONS.